nature communications

Article

https://doi.org/10.1038/s41467-025-62544-w

Adaptive loss of shortwave-sensitive opsins during cartilaginous fish evolution

Received: 24 July 2024

Accepted: 22 July 2025

Published online: 18 August 2025

Check for updates

Bo Zhang[1,2,7], Yidong Feng[1,7], Meiqi Lv[3,7], Lei Jia[4], Yongguan Liao[1], Xiaoyan Xu[1], Axel Meyer[5], Jinsheng Sun[4], Guangyi Fan[6], Yumin Li[1], Yaolei Zhang[3] ✉, Na Zhao[2] ✉, Yunkai Li[1] ✉ & Baolong Bao[1] ✉

Cartilaginous fishes (e.g., sharks, rays, and skates) cannot see blue or violet light, potentially because they lack the shortwave-sensitive cone opsin gene (*sws*). Widespread gene loss can occur during evolution, but the evolutionary mechanisms underlying *sws* loss remains unclear. Here, we construct whole-genome assemblies of *Okamejei kenojei* (skate) and *Prionace glauca* (blue shark). We then analyze the distribution characteristics and intragroup differences of opsin-related genes in cartilaginous fishes. Using a zebrafish model with *sws* deleted we infer that in the presence of SWS1 and SWS2, blue and violet light respectively, can induce cell aging. This is followed by photoreceptor layer thinning, demonstrating, *sws* loss aids in preventing shortwave light damage to the eye. In the retinas of numerous cartilaginous fishes, the tapetum lucidum strongly reflects light. Therefore, in cartilaginous fish, the existence of tapetum lucidum in the retina and loss of *sws* may be interdependent; in other words, this adaptive gene loss may increase cartilaginous fish fitness.

Visual perception is essential in animals; it conveys the color, shape, size, and movement of their surrounding objects and aids them in responding to changes in the surrounding environment. An animal's visual capability depends on its opsin genes. In vertebrates, opsins include a rod opsin (RH1), which provides low-light visibility, and four classes of cone opsins (SWS1, SWS2, RH2, and LWS), which facilitate visibility in bright light and detection of colors across the visible light spectrum. In many species, these opsins have undergone alterations, loss, or duplication throughout evolution, which has provided them with unique adaptations enabling underwater vision. Agnathan (jawless) lampreys demonstrate the full complement of one rod and four cone opsin genes[1]; however, they may have lost the shortwave sensitive cone opsin genes *sws*1 and *sws*2 before the divergence of the holocephalans (chimeras) and elasmobranchs (sharks, skates, and rays)[2]. Ancestral chondrichthyans retained only the green-light-sensitive cone opsin gene (*rh2*), and the long-wavelength–sensitive cone opsin gene (*lws*) with all cartilaginous fishes losing *sws*1 and *sws*2.

Among elasmobranchs, sharks (Selachii) have retained only *rh1* and one cone opsin gene; as such, they may be cone monochromats, lacking the ability to see colors. Moreover, rays (Batoidea) have retained *rh1* and two cone opsin genes *rh2* and *lws* and thus may have dichromatic color vision[3–5]. In particular, behavioral experiments have revealed that giant shovelnose rays can discriminate color[6]. However, data regarding cone pigments and color vision in the other major batoid groups, including skates and sawfishes, remain unavailable; nevertheless, at least two skate species may possess rod-only retinae[7].

Since the sequencing of the elephant shark genome, several whole-genome sequences of cartilaginous fishes, such as whale sharks, brown-banded bamboo sharks, and cloudy catsharks[8–10], have been reported. They provide genome-level data outlining the elasmobranch

[1]International Research Center for Marine Biosciences, Ministry of Science and Technology, Shanghai Ocean University, Shanghai 201306, China. [2]Southern Marine Science and Engineering Guangdong Laboratory-Zhanjiang, Zhanjiang 524000, China. [3]BGI Research, Qingdao 266555, China. [4]Tianjin Fisheries Research Institute, Tianjin 300200, China. [5]Lehrstuhl für Zoologie und Evolutionsbiologie, Department of Biology, University of Konstanz, Konstanz, Germany. [6]State Key Laboratory of Genome and Multi-omics Technologies, BGI Research Shenzhen, Shenzhen 518083, China. [7]These authors contributed equally: Bo Zhang, Yidong Feng, Meiqi Lv. ✉e-mail: zhangyaolei@genomics.cn; penguinzn@163.com; ykli@shou.edu.cn; blbao@shou.edu.cn

opsin evolution. However, additional whole-genome sequences, particularly those of the skate genome, are required to obtain a more detailed representation of elasmobranch opsin evolution. Moreover, evolutionary mechanisms underlying SWS loss remain unclear. Here, we perform whole-genome analyses of the skate (*Okamejei kenojei*), a cold temperate near-bottom–dwelling cartilaginous fish in East Asia, and the blue shark (*Prionace glauca*), the currently most hunted oceanic shark species found in temperate and tropical waters globally. We also perform combined gene functional analysis to obtain an in-depth explanation of opsin gene evolution in cartilaginous fishes.

Results

Genome sequences and assembly

We constructed a PacBio continuous long reads (CLRs) library for *O. kenojei* and a circular consensus sequencing (CCS) library for *P. glauca*, generating sequencing data with 232.59- and 91.22-Gb of long reads, respectively. Whole-genome short-reads and Hi-C sequencing were also performed for initial contig assembly polishing and chromosome anchoring (Supplementary Table 1). The *O. kenojei* and *P. glauca* genomes were assembled to be 2.75 and 3.23 Gb long (Supplementary Table 2)—similar to the K-mer estimation results from 17mer analysis (i.e., 2.79 and 3.25 Gb; Supplementary Fig. 1); moreover, the contig N50 lengths were 1.50 and 5.32 Mb (Supplementary Table 2), and the BUSCO scores were 94.8% and 94.0% based on Core Vertebrate Genes in GVolante (https://gvolante.riken.jp/), and 93.9% and 91.9% based on metazoa_odb10 datasets, respectively (Supplementary Table 3), comparable to that for other chondrichthyans (Supplementary Fig. 2). These results revealed good assembly continuity and gene completeness. Incorporating the Hi-C data, approximately 96.28% (2.65 Gb) and approximately 97.85% (3.16 Gb) of the assembled contigs were anchored to 44 and 43 chromosomes, respectively (Supplementary Fig. 1). Additionally, 22,965 and 21,229 protein-coding genes were predicted in *O. kenojei* and *P. glauca* genomes, with approximately 97.01% and approximately 98.87% of them functionally annotated based on public databases, respectively (Supplementary Table 4).

Transposable elements

Repetitive sequences in a genome have critical roles, such as gene expression regulation, in driving evolution[11]. Moreover, the proportion of repetitive sequences in cartilaginous fish genomes is relatively higher than that in most teleosts[12,13]. Therefore, we included all available cartilaginous fish genomes published thus far and detected repetitive sequences by using identical pipelines to achieve an in-depth view of repetitive sequence evolution. In general, we observed that transposable elements (TEs) accounted for approximately 69.27% and 66.44% of the *O. kenojei* and *P. glauca* genomes, respectively (Supplementary Table 5 and 6), which did not demonstrate significant differences compared with other cartilaginous fish genomes (Fig. 1a). However, skates (3.28%) and rays (2.30%) demonstrated significantly higher average proportions of the DNA transposon subtype TcMar (Tc1/mariner) elements than sharks (0.14%) and chimaera (0.03%; Fig. 1b). TcMar includes several subcategories, including TcMar-piggyBac, TcMar-Sleeping Beauty (SB), TcMar-ZB, TcMar-Mos1, and TcMar-Passport, widely distributed in vertebrate genomes. These TEs are powerful tools for genetic manipulation in various species, including zebrafish, *Caenorhabditis elegans*, and mice, and they have an apparent preference for insertion into genes and transcriptional regulatory regions of genes[14–18]; thus, the TEs may contribute considerably to the genome evolution and unique characters of a species. Moreover, sharks and chimaeras have a body shape similar to a typical fish, whereas most skates and rays exhibit a flattened body with wing-like fins; however, only *Pristis pectinata* have bodies shaped similar to sharks with fins slightly shaped similar to wings, which are not as obvious as those of other skates and rays. Notably, the proportion of TcMar (0.33%) in the *P. pectinata* genome was slightly higher than that in sharks and chimaeras but significantly lower than that in skates and rays with wing-like fins. Consequently, we hypothesized that an increase in TcMar expression may affect body shape development in skate and rays through regulation of related genes or regulator activation.

Next, we investigated the genes whose locus overlapped with TcMar element blocks in these cartilaginous fish genomes. Notably, we identified 3530 genes shared by skates and rays, which is significantly greater than other DNA transposons types (Supplementary Data 1 and Supplementary Fig. 3), but only 28 genes shared by sharks and chimaeras. The results of our Kyoto Encyclopedia of Genes and Genomes (KEGG) pathway enrichment analysis demonstrated that all 3,530 genes were significantly enriched in 73 pathways ($q < 0.05$), including the cell cycle, GnRH signaling pathway, citrate cycle (TCA cycle), and B-cell receptor signaling pathway (Supplementary Data 2); these pathways are crucial for maintaining life activities. In particular, 60 genes were enriched in the Wnt pathway ($q = 1.82 \times 10^{-6}$), a highly conserved system critical to the patterning of the entire body plan, regulating complex biological processes including controlling axis elongation and cell migration to specific locations[19,20]. These 60 genes included *wnt2/3/5/7/9*, *axin1*, *gsk3b*, *dvl1*, *fzd6*, *lrp6*, *ror1/2*, and *lef1*, which play integral roles in the WNT pathway. The WNT/PCP (planar cell polarity) pathway is a key contributor to skate fin morphology[21]. Therefore, the regulatory expression of genes determines the process of this signaling pathway, and TcMar elements may regulate gene expression, particularly because they are expanded in most skates and rays (Fig. 1c) and regulate the aforementioned important genes. Moreover, we found three rounds of expansion events in skates and at least one round of expansion in rays, indicating innovation in the species (Fig. 1d).

Frequent interchromosomal rearrangements in cartilaginous fishes

Karyotypes can vary considerably among cartilaginous fishes; this has attracted considerable research attention[13,21]. However, chromosomal changes across cartilaginous fishes have been noted and systematically compared thus far. Thus, we elucidated syntenic relationships among the published chromosomal-level assemblies of four skate, three ray, eight shark, and one chimaera species to assess chromosome rearrangement changes among cartilaginous fishes. We observed an overall conserved pattern of synteny blocks across all genomes but noted abundant interchromosomal rearrangement events between different orders (Fig. 1e). In the superorder Batoidea, the chromosomes of skate species maintain one-to-one correspondence. In contrast, many chromosome fusions were noted in the ray species *Hypanus sabinus* and *Mobula birostris* from the order Myliobatiformes: chr2–chr26, chr1–chr6, chr9–chr14, chr4–chr38, chr7–chr12, chr3–chr18, chr21–chr25, chr28–chr36, chr35–chr39, and chr41–chr44. These fusions led to a rapid reduction of chromosome numbers of the ray species. In the superorder Batoidea, seven chromosomes (i.e., chr17, chr23, chr27, chr32, chr15, chr33, and chr29) maintained a stable one-to-one chromosome synteny overall, whereas 15 chromosomes (i.e., chr1, chr2, chr6, chr9, chr14, chr38, chr4, chr7, chr12, chr8, chr3, chr20, chr22, chr13, and chr19) demonstrated more than two fusion and fission events (Fig. 1e). Among the sharks, *Squalus acanthias*, with relatively few chromosomes, exhibited multiple chromosome fusion events but demonstrated an excellent syntenic relationship with Orectolobiformes sharks. In contrast, in Carcharhiniformes and Lamniformes sharks, frequent chromosomal rearrangement events were noted. Only chr7 and chr34 were in a stable one-to-one collinear relationship among the shark and chimaera species, whereas 14 chromosomes (i.e., chr3, chr12, chr9, chr8, chr19, chr16, chr14, chr4, chr27, chr20, chr23, chr30, chr24, and chr28) demonstrated more than two fusion and fission events. Moreover, in cartilaginous fish, sex

https://doi.org/10.1038/s41467-025-62544-w

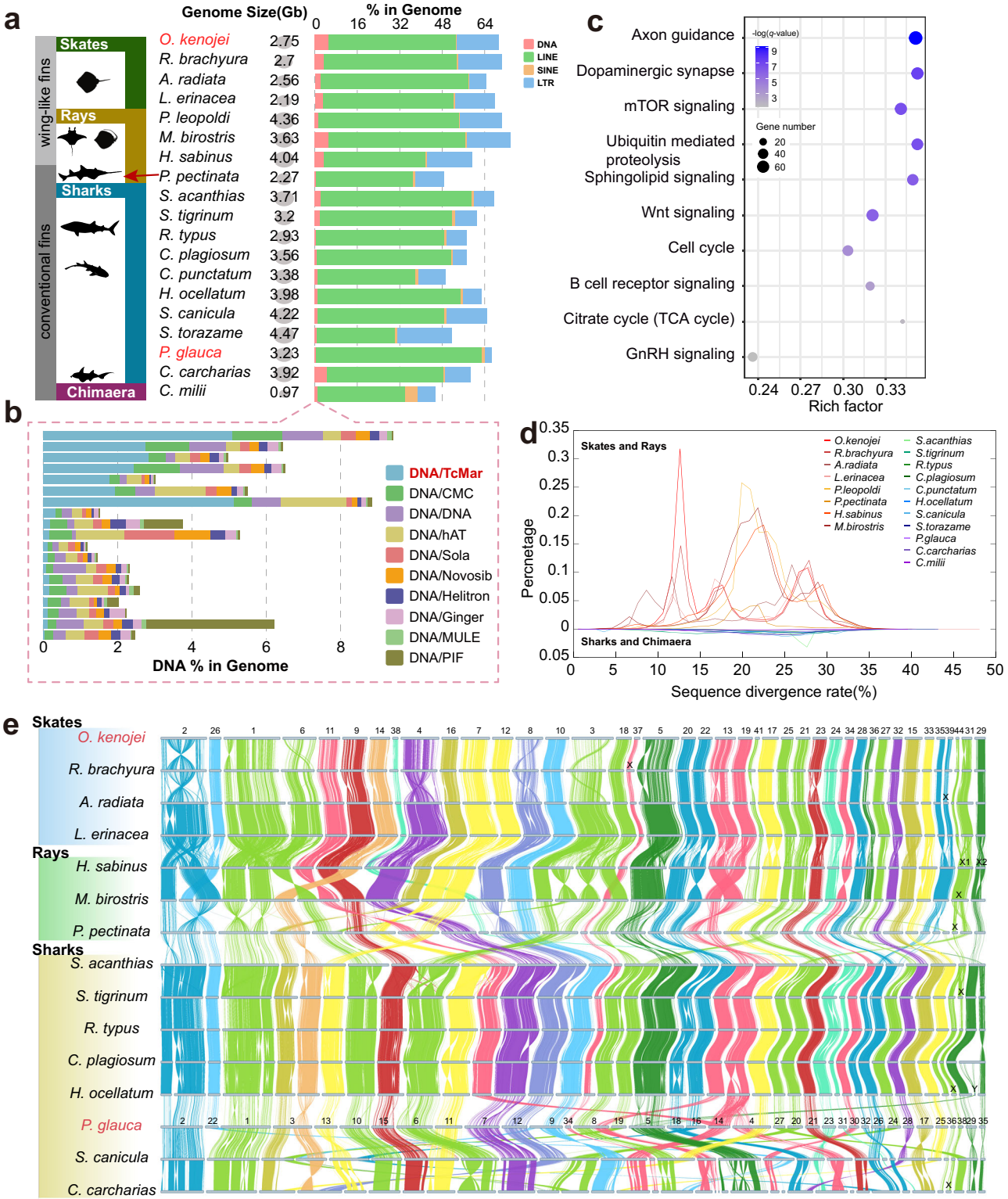

Fig. 1 | Genomic characteristics of cartilaginous fishes. a Genome sizes and proportions of DNA transposons, LINEs, SINEs, and LTRs in cartilaginous fish genomes. **b** Top 10 abundant TE superfamilies of cartilaginous fishes. **c** Top 10 KEGG pathways of overlapped TcMar element blocks in cartilaginous fish genomes, including 3,530 genes shared by skates and rays but only 28 genes shared by sharks and chimaeras. **d** Divergence rates of Tc1/mariner TEs in cartilaginous fish genomes. **e** Pairwise whole-genome alignments across 15 chromosome-level assemblies of cartilaginous fishes. Each bar represents a chromosome, and the labels on top denote the chromosome IDs.

chromosomes may not have originated from the same ancestral chromosome, and multiple rearrangement events occurred between the sex chromosomes and autosomes. These chromosome arrangements may be related to the genome size changes due to an increase in the number of repetitive sequences, resulting in chromosome instability.

To determine the phylogenetic relationships for our newly sequenced species, we performed gene family analysis on 17

representative species, including skate and shark species, and 8 teleosts. By using SonicParanoid, we identified 10,010 single-copy orthologous genes and 335 of them were one-to-one genes in these 17 species. Then we constructed a phylogenetic tree using the maximum-likelihood method based on the 14,009 fourfold degenerate sites sampled from the 335 genes and found that *O. kenojei* is unequivocally clustered with *Amblyraja radiata*, and *P. glauca* is the sister branch of *Scyliorhinus torazame* (Supplementary Data 3). We also elucidated the evolutionary relationships among other species used in our analysis; the results were consistent with published studies[13], confirming their reliability. We then inferred divergence times with 10 fossil times from the TimeTree database[22]: the skates separated from the sharks about 259 million years ago (Mya; Fig. 2a)—also in line with previous results[23]. *O. kenojei* diverged from *A. radiata* approximately 33.9 Mya, whereas *P. glauca* diverged from *S. torazame* approximately 103.4 Mya.

Expanded gene families in the two novel genomes

Gene family expansion often plays a critical role in biological diversity, adaptability, and complexity of organisms[24,25], thus we conducted related analysis for the newly assembled genomes, identifying 311 and 444 expanded gene families (Supplementary Data 4), as well as 233 and 133 contracted gene families (Supplementary Data 5) in *O. kenojei* and *P. glauca*, respectively (Fig. 2a). In *O. kenojei*, the expanded gene families including 1,246 genes were mainly enriched in pathways related to survival adaptations, including carbohydrate metabolism, signal transduction, as well as the endocrine, immune, and sensory systems (Fig. 2b). In *P. glauca*, 444 expanded gene families including 1,611 genes were enriched in pathways mostly different from those in *O. kenojei* (Fig. 2c). Nevertheless, most of these genes were related to the immune and endocrine systems and signal transduction. We found that although *O. kenojei* and *P. glauca* both enriched in the same immune pathway, the specific genes undergoing expansion might be different (Supplementary Data 4). For instance, in the RIG-I-like receptor signaling pathway, previous study showed that RIG-like receptors themselves are conserved in gene copy number[26]. However, genes acting within this pathway, such as tumor necrosis factor (TNF) and interferon alpha (*IFNA*), exhibit increased copy numbers in *O. kenojei* and *P. glauca*, respectively, as shown in Supplementary Fig. 4a, b, suggesting the expansion of different gene families might reflect species-specific requirements in responding to environmental pressures. Moreover, one of the pathways in *P. glauca* was related to ovarian steroidogenesis, through which ovarian cells produce hormones regulating ovarian function and ovulation[27]. *P. glauca* is viviparous with super-reproductive capabilities. At each breeding, it can produce an average of 30–50 pups (with the highest being 135 pups)—much higher than that produced by other cartilaginous fishes in the open ocean globally[28]. We found that in *P. glauca*, there is one more copy of the STAR gene which encodes steroidogenic acute regulatory protein (StAR) compared to other cartilaginous fishes. StAR is a cholesterol-transporting protein which is important in steroid hormone biosynthesis[29,30] and potentially contributes to multiple births for *P. glauca*.

Sensory gene repertories

Vertebrates have developed five visual pigment opsin gene lineages, including four distinct cone opsins (i.e., *lws*, *sws1*, *sws2*, and *rh2*) expressed in cone cells and one rod opsin (*rh1*) expressed in rod photoreceptors[31]. We noted that skates lost *lws* and *rh2*, whereas these genes were retained in sharks and rays (Fig. 2d and Supplementary Fig. 5). We didn't identify *sws1* and *sws2* in all assembled cartilaginous fish genomes (Fig. 2d), consistent with previous results[10], which may suggest these two gene losses are ancestral events. We noted good retention of the gene block (with or without *sws1*) in both the cartilaginous and bony fishes (Fig. 2e), but *sws1* was lost in cartilaginous fishes. However, *sws*2 was likely lost because of considerable changes due to chromosome rearrangements; compared with the bony fishes, the cartilaginous fishes did not demonstrate any gene collinearity or blocks (Fig. 2f). Cartilaginous fishes may have evolved other more advanced sensory systems, and *sws1* and *sws2* loss may be adaptive or regressive. Thus, we performed a series of experiments to explore the mechanisms underlying *sws1* and *sws2* loss.

SWS-dependent shortwave-light-induced retina injury

Several selection pressures may have led to a universal SWS loss in cartilaginous fishes. We hypothesized that these fishes demonstrate SWS-dependent shortwave-light–induced retina injury. Compared with white light, we found that shortwave blue or violet light led to considerable injury to the retina in zebrafish after one month of irradiation, showing fewer photoreceptor cells, as well as shorter photoreceptor and pigment epithelial cell layers. However, longwave red or yellow-green light did not cause these injuries. Moreover, no injury was noted in other layers, including the outer nuclear, outer plexus, inner nuclear, inner plexus, and nerve fiber layers (Supplementary Fig. 6a, b).

In our comparative transcriptomic analysis with white light irradiation, irradiation with shortwave light including blue and violet light co-upregulated the expression of 176 apoptosis-related genes and 167 cell aging-related genes (Supplementary Fig. 7a, Supplementary Data 6); thus, shortwave light might cause cell apoptosis and aging in eyes. Our quantitative reverse transcription polymerase chain reaction (RT-qPCR) results revealed that shortwave irradiation upregulated marker genes related to apoptosis (*caspase3b* and *p21* genes) and cell aging (*mmp65* and *il6*) in zebrafish eyes (Supplementary Fig. 7b). Immunohistochemically staining for Caspase3b and Il6 confirmed these results (Supplementary Fig. 7c). TUNEL staining confirmed the presence of DNA breaks in zebrafish retinas (Supplementary Fig. 7d), this result was corroborated by that of a previous result, which was due to high-energy blue light inducing and accelerating cellular damage through apoptosis[32,33].

To determine whether shortwave-light–induced eye injuries may depend on shortwave sensitive opsins, we established *sws1*$^{-/-}$ and *sws2*$^{-/-}$ mutants (*sws1* official name: *opn1sw1*, *sws2* official name: *opn1sw2*) of zebrafish by using the CRISPR/Cas9 genome editing technology, and the behavior testing results demonstrated that the mutants had lost the ability to detect shortwave light (Supplementary Fig. 8). After shortwave light irradiation, the photoreceptor cell layer was thicker, with more, longer photoreceptor cells, in both the *sws1*$^{-/-}$ and *sws2*$^{-/-}$ mutants of zebrafish than that in the wild-type (WT) zebrafish (Fig. 3a). This result indicated that shortwave-light-induced injury in photoreceptor cells depends on SWS1 and SWS2. Furthermore, shortwave light irradiation led to up regulation of 94 and 97 downregulation of 97 and 92 cell-aging-related genes in the eyes in the *sws2*$^{-/-}$ and *sws1*$^{-/-}$ mutants, respectively (Fig. 3b, Supplementary Data 7). The relative expression of the two cell aging marker genes *p16* and *il6* was significantly lower in the *sws*$^{-/-}$ mutant than in the WT, indicating that cell aging might play a major role in photoreceptor cell injury. Immunofluorescence staining demonstrated a significantly low signal for P16 in the retina of both the *sws1*$^{-/-}$ and *sws2*$^{-/-}$ mutants, further confirming the aforementioned observations (Fig. 3c).

SWS-dependent shortwave-light–induced injury can cause cell aging via photoreceptor layer thinning, which is also a biomarker for age-related macular degeneration (AMD). AMD, a leading cause of vision loss in humans[34], can result from excessive exposure to blue light received during an individual's entire lifespan[35,36]. To further confirm whether shortwave-light–induced cell aging depends on SWS in zebrafish or humans, we overexpressed zebrafish *sws*1 and *sws*2 and human *sws* in HEK293 cells (Supplementary Fig. 9). Senescence-associated β-galactosidase (SA-β-gal) staining demonstrated a strong β-galactosidase signal in *sws*-overexpressing cells, confirming that the cells were aging (Fig. 4a). Moreover, *sws*-overexpressing cells exhibited strong P16 signals (Fig. 4b). These results further confirmed that cell

https://doi.org/10.1038/s41467-025-62544-w

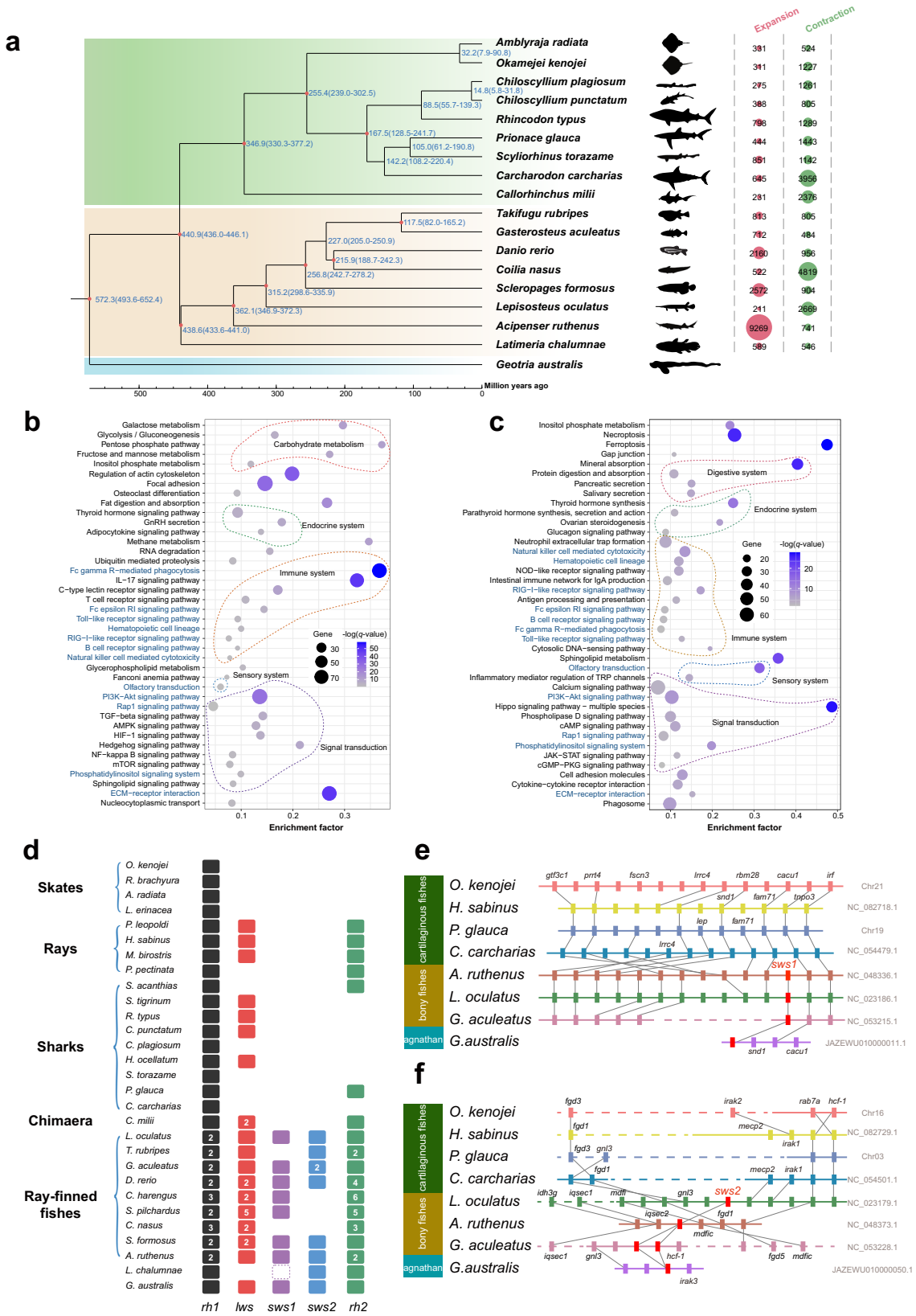

Fig. 2 | Phylogeny and comparative genomics of cartilaginous fishes. **a** Phylogenetic and gene family expansion and contraction analysis of *O. kenojei* and *P. glauca*. **b**, **c** KEGG pathway enrichment analysis of expanded genes in *O. kenojei* (**b**) and *P. glauca* (**c**). Top 40 enriched pathways are shown; the pathways labeled in blue are shared by both species. **d** Orthology catalog for opsins in cartilaginous fishes. The numbers in the boxes are paralog numbers; the dashed box represents a pseudogene. **e**, **f** Loss of *sws1* (**e**) and *sws2* (**f**) in cartilaginous fishes, respectively. Synteny of genes around *sws1* and *sws2* is illustrated using gray bands connecting the orthologs across species (The dashed lines indicate that these two genes are not adjacent on the scaffold or chromosome).

https://doi.org/10.1038/s41467-025-62544-w

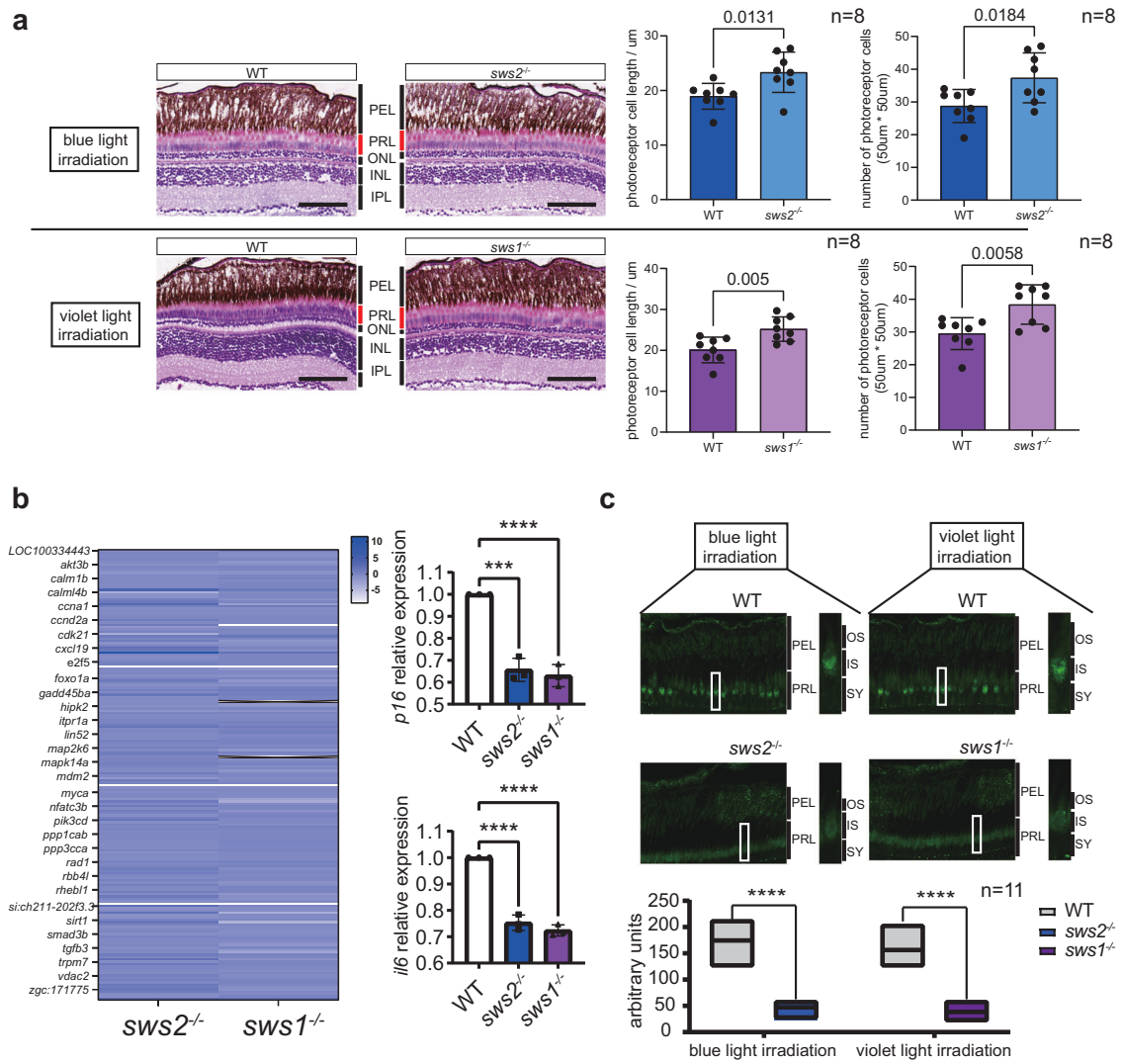

Fig. 3 | SWS-dependent retina injury and cell aging in zebrafish eyes after shortwave light irradiation. a Statistical results of the numbers and lengths of photoreceptor cells in wild type (WT) and *sws2*$^{-/-}$ zebrafish after exposure to blue (λ_{max} = 420 nm) and violet (λ_{max} = 370 nm) light. Two-sample two-sided unpaired t test: $p = 0.0131$, 95% CI = [1.081, 7.737], mean diff. = 4.409 ± 1.552, $df = 14$, $t = 2.841$, $R^2 = 0.3657$; $p = 0.0184$, 95% CI = [1.691, 15.56], mean diff. = 8.625 ± 3.233, $df = 14$, $t = 2.668$, $R^2 = 0.3370$; $p = 0.0050$, 95% CI = [1.806, 8.379], mean diff. = 5.093 ± 1.533, $df = 14$, $t = 3.323$, $R^2 = 0.4409$; $p = 0.0058$, 95% CI = [3.016, 14.73], mean diff. = 8.875 ± 2.732, $df = 14$, $t = 3.249$, $R^2 = 0.4299$. Data are from 8 samples per group, no adjustments were made for multiple comparisons. Data are representative of three independent experiments. Source data are provided as a Source Data file. **b** Transcriptomic expression heatmaps of *sws2*$^{-/-}$ compared to WT zebrafish exposed to blue light, and of *sws1*$^{-/-}$ compared to WT zebrafish after violet light irradiation. In total, 94 and 97 cell-aging-related genes were upregulated, 97 and 92 genes were down regulated in the *sws2*$^{-/-}$ and *sws1*$^{-/-}$ mutants, respectively. Some of the cell-aging-related genes are shown in the Y-axis. One-way ANOVA: $F(2, 6) = 71.87$, $p < 0.0001$, $R^2 = 0.9599$; Dunnett's multiple comparisons test: WT vs. *sws2*$^{-/-}$: mean diff. = 0.3434, 95% CI = [0.2448, 0.4420], adjusted $p = 0.0001$, ***; WT vs. *sws1*$^{-/-}$: mean diff. = 0.3701, 95% CI = [0.2716, 0.4687], adjusted $p < 0.0001$, ****.One-way ANOVA: $F(2, 6) = 160.1$, $p < 0.0001$, $R^2 = 0.9816$; Dunnett's multiple comparisons test: WT vs. *sws2*$^{-/-}$: mean diff. = 0.2470, 95% CI = [0.1984, 0.2956], adjusted $p < 0.0001$, ****; WT vs. *sws1*$^{-/-}$: mean diff. = 0.2762, 95% CI = [0.2276, 0.3247], adjusted $p < 0.0001$, ****. Data are from 3 replicates per group and representative of three independent experiments. Source data are provided as a Source Data file. **c** Immunofluorescent signal for P16 in the inner segment of the retina. Two-sample two-sided unpaired t test: $p < 0.0001$, 95% CI = [−144.7, −105.1], mean diff. = −124.9 ± 9.492, $df = 20$, $t = 13.16$, $R^2 = 0.8965$; two-sample two-sided unpaired t test: $p < 0.0001$, 95% CI = [−132.9, −93.42], mean diff. = −113.2 ± 9.474, $df = 20$, $t = 11.95$, $R^2 = 0.8771$. Data are from 11 samples per group and representative of three independent experiments, no adjustments were made for multiple comparisons. Source data are provided as a Source Data file. PEL pigment epithelial layer, PRL photoreceptor layer, ONL outer nuclear layer, INL inner nuclear layer, IPL inner plexiform layer, OS outer segment, IS inner segment, SY synapse.

aging induced by shortwave light depends on SWS of zebrafish or human.

Discussion

Whole-genome sequencing of cartilaginous fish can facilitate the exploration of vertebrate evolution[8–10]. Here, we assembled high-quality chromosomal-level genomes of two cartilaginous fish and discovered a series of crucial evolutionary events. First, the diversity and evolution of TEs, major vertebrate genome components, have been studied widely. In general, the genome TE content is higher in cartilaginous fish (45.65–74.79%) than in bony fish (5–56%)[37]. Cartilaginous fish exhibit similar repeat sequence compositions; of all repeat sequences, 86.68–97.78% are LINE and LTR, the two main repeat sequence types. However, we found that repeat subtypes in skates and rays differed from those in sharks and chimaeras; these subtypes included TcMar, which may be critical in determining the body plan.

Chromosomal evolutionary events, such as whole-genome duplication and rearrangements, are of great significance to the

https://doi.org/10.1038/s41467-025-62544-w

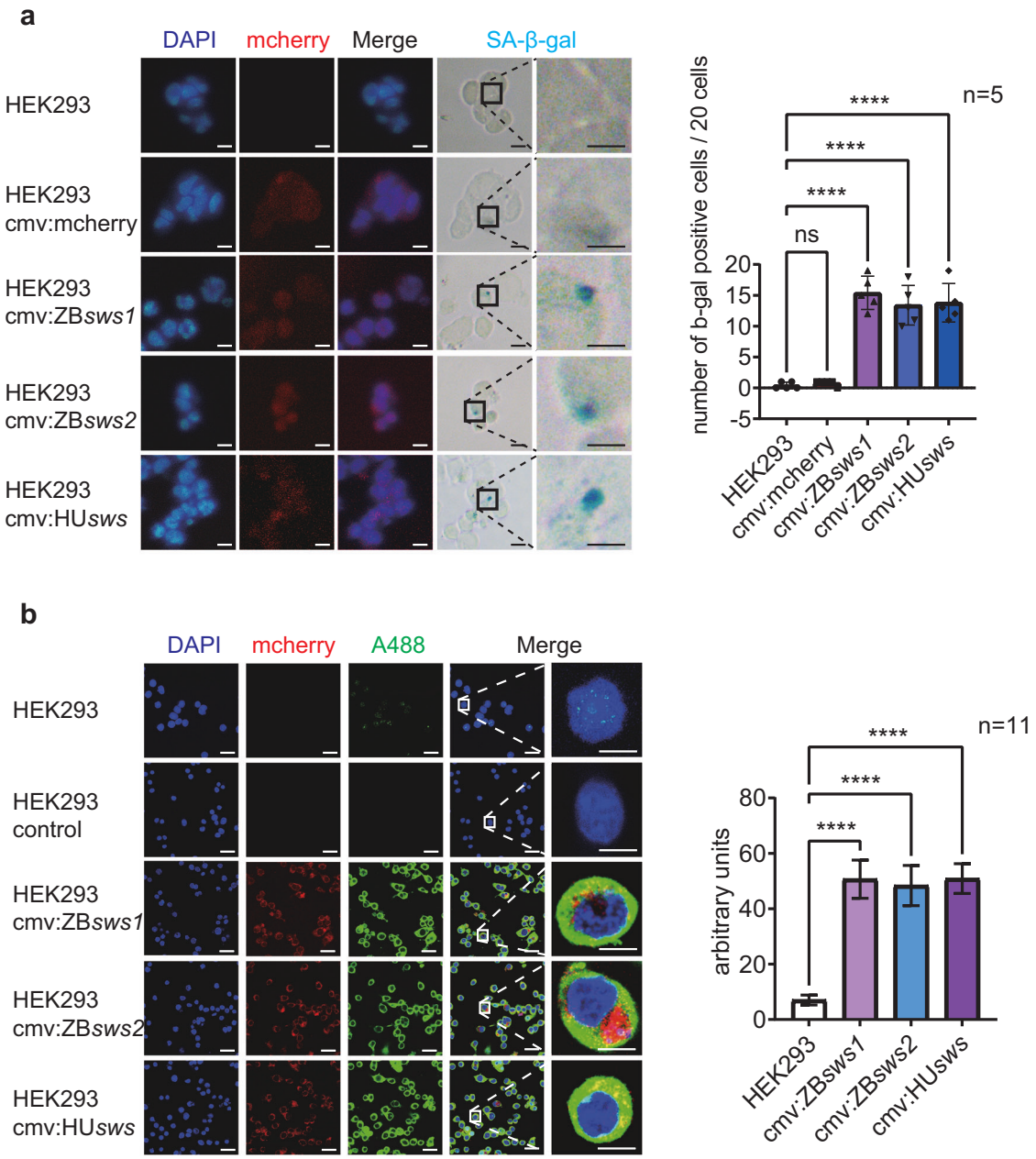

Fig. 4 | Cell aging detection in *sws*-overexpressing HEK293 cells. a. SA-β-gal staining of cells overexpressing mcherry, zebrafish *sws1*, zebrafish *sws2*, or human *sws* (i.e., blue precipitate). SA-β-gal was not observed in the untransfected HEK293 cells and HEK293 control (cmv:mcherry) cells. Scale bar: 10 μm. Twenty cells were randomly selected from each section to count the number of SA-β-gal positive cells. One-way ANOVA: $F(4, 20) = 50.42$, $p < 0.0001$, $R^2 = 0.9098$; Dunnett's multiple comparisons test: HEK293 vs. cmv:mcherry: mean diff. = −0.4000, 95% CI = [−4.354, 3.554], adjusted $p = 0.9962$, ns; HEK293 vs. cmv:ZB*sws1*: mean diff. = −15.00, 95% CI = [−18.95, −11.05], adjusted $p < 0.0001$, ****; HEK293 vs. cmv:ZB*sws2*: mean diff. = −13.00, 95% CI = [−16.95, −9.046], adjusted $p < 0.0001$, ****; HEK293 vs. cmv:HU*sws*: mean diff. = −13.40, 95% CI = [−17.35, −9.446], adjusted $p < 0.0001$, ****. Data are from 5 replicates per group and representative of three independent experiments. Source data are provided as a Source Data file. **b**. Immunofluorescence detection of P16 through confocal microscopy. The negative control group comprised HEK293 cells not exposed to primary antibodies. Scale bar: 10 μm. One-way ANOVA: $F(3, 40) = 153.6$, $p < 0.0001$, $R^2 = 0.9201$; Dunnett's multiple comparisons test: HEK293 vs. cmv:ZB*sws1*: mean diff. = −43.63, 95% CI = [−49.62, −37.64], adjusted $p < 0.0001$, ****; HEK293 vs. cmv:ZB*sws2*: mean diff. = −41.31, 95% CI = [−47.30, −35.32], adjusted $p < 0.0001$, ****; HEK293 vs. cmv:HU*sws*: mean diff. = −43.84, 95% CI = [−49.82, −37.85], adjusted $p < 0.0001$, ****. Data are from 11 replicates per group and representative of three independent experiments.Source data are provided as a Source Data file.

speciation and shaping of new features in species. Although gene duplication and its adaptive significance have been discussed widely, gene loss has been much less studied. Both gene loss and gain play major roles in animal evolution[24,25,38,39]. Similar to the published genomes of several other cartilaginous fish, our skate (*O. kenojei*) and blue shark (*P. glauca*) genomes demonstrated *sws* loss. Inability to sense shortwave light in sharks has been a topic of shark genome research[10,40,41]. Two main molecular mechanisms may underlie the loss of a gene from a genome: an abrupt mutational event or slow mutation accumulation during pseudogenization[42]. Our comparative genomics analysis revealed no *sws1* and *sws2* pseudogene among the cartilaginous fish genomes (Fig. 2d), indicating that *sws* was more likely lost because of substantial changes, such as chromosome rearrangements (Fig. 2e, f). However, because we included a limited number of cartilaginous fish species here, we could not rule out that *sws1* loss in cartilaginous fish exemplified whole gene deletion based on partial

functional loss due to mutations or pseudogenization. In some bony fish[43] and bats[44], *sws1* has undergone different degrees of mutation or pseudogenization. Because *sws* loss was noted in all cartilaginous fish (Fig. 2d), *sws* may have been lost 360 Mya before the divergence of the holocephalan (chimeras) and elasmobranchs (sharks, skates, and rays; Fig. 2a)[29]. In other words, *sws* loss occurred in the common ancestors of chondrichthyans before subclass formation—much earlier than the mass extinction that preceded the species extinction 66 Mya[45], as well as mass extinction 19 Mya when >90% of shark species disappeared[46].

Because neither SWS1 nor SWS2 exists in their retina, cartilaginous fish cannot see blue or violet light in their surrounding optic environment. Thus, *sws* loss may not have occurred stochastically but due to gene function loss in cartilaginous fish. Here, we noted that shortwave-light–induced injury may depend on SWS; violet or blue light via SWS1 or SWS2 caused photoreceptor layer thinning via cell aging in zebrafish; in contrast, red or yellow light irradiation had no such effect. Moreover, shortwave light induced cell aging in cells overexpressing zebrafish *sws*. Therefore, *sws* loss may be associated with a decrease in retinal injury.

Cartilaginous fishes[47–50] such as skates (*O. kenojei*) and blue sharks (*P. glauca*) have tapeta lucida in the choroid behind the retina (Fig. 5a). The tapetum consists of a single layer of guanophores—highly reflective, plate-like cells—which doubles the optical path length of the photoreceptor outer segments and consequently increases eye sensitivity[48]. Without *sws* loss, tapeta lucida behind the retina would have worsened SWS-dependent eye injury in cartilaginous fish (Fig. 5b).

Gene loss with neutral effects on fitness can occur during regressive evolution. For instance, the loss of the *oca2* gene has allowed *Astyanax cavefish* to adapt to life in the perpetual darkness of caves, without any apparent deleterious effects[51]. Moreover, seahorses (lacking pelvic fins) lost *tbx4*, a hindlimb development regulator gene, over time[52]. In cartilaginous fish, *sws* loss may not represent regressive evolution, but it may follow the less-is-more hypothesis, noted in populations exposed to changes in selective pressure patterns because of considerable shifts in environmental conditions[53,54]. Tapeta lucida do not occur in amphioxi or agnathans; as such, the guanine choroidal tapetum may have arisen in sharks, sturgeon, and lobe-finned fish independent of each other, potentially to allow them to explore deeper and darker parts of the ocean[55]. Cartilaginous fish species that gradually spread from deeper parts of the ocean into the epipelagic zone (with multispectrum light prevalent) may have lost *sws* to prevent retina injury. In shallow waters or ocean surfaces, *lws* or *rh* can meet the vision requirements of cartilaginous fish. This is the first study to explain and assess the mechanism of adaptive gene loss in cartilaginous fish. Nevertheless, adaptive gene loss according to the less-is-more hypothesis has been described in flies, whereby positive selection associated with colonization of new ecological niches led to accelerated loss of some chemoreceptors genes[56]. The loss of *KLK8* (involved in sweat gland and hippocampus development) has led to epidermis thickening, hair loss, and reduced water resistance in Cetaceans, aiding marine environment adaptation[39,57].

In the presence of SWS, both blue and violet light can engender cell aging, leading to photoreceptor layer thinning in zebrafish. Moreover, photoreceptor layer thinning is an AMD biomarker in humans[34]. Our results indicated that blue light can induce aging in HEK293 cells overexpressing human *sws*, supporting the possible role of blue light in AMD development. Although AMD is a major health issue in the developed world, accounting for approximately half of all blind registrations, no AMD-related gene has been reported so far. Thus, our findings may facilitate future screenings for AMD marker genes associated with SWS-dependent transduction and downstream signaling pathways (e.g., cell aging).

Methods

Ethics statement

All animal experiments and field work were conducted according to the standard animal guidelines approved by the Animal Care Committee of Shanghai Ocean University (Approval No. SHOU-DW-2021-011).

DNA and RNA sequencing

O. kenojei were caught at Bohai Bay in China, and genomic DNA was extracted from their muscle tissues. A short-read paired-end library with a 350-bp insert size was sequenced on the BGISEQ-500 platform (BGI Qingdao, China), and two 20-kb-long read libraries were constructed and sequenced on the RSII platform (Pacific Biosciences, California, USA) in the CLR mode, according to the official standard protocol. For Hi-C sequencing, libraries were constructed and sequenced on the BGISEQ-500 platform with 100-bp paired-end reads, according to the official standard protocol[58]. RNAs were extracted from six tissues, including the eye, ovarium, dorsal skin, abdomen skin, liver, and spermary, by using a TRIzol kit (Invitrogen, USA), and the libraries were sequenced on the BGISEQ-500 platform (Supplementary Table 7). For *P. glauca*, caught from the western Pacific Ocean, we constructed a short-read 350-bp library and sequenced it on the Illumina Novaseq platform. Genomic DNA was broken down into approximately 15-kb-long fragments to construct a long-read library and sequenced on the PacBio Sequel II platform in the CCS mode.

Genome assembly and chromosome anchoring

SMARTdenovo[59] was used to assemble the *O. kenojei* genome by using long reads with default parameters. Then, the contigs were polished using Pilon (version 1.22)[60] by using the clean short reads filtered using Soapnuke (version 1.6.5) with these parameters: -M 1 -A 0.4 -d -n 0.02 -l 10 -q 0.1 -Q 2 -G. Finally, the Hi-C data were mapped to the draft genome by using Juicer[61] and anchored to the chromosome using the 3D-DNA pipeline[62]. For the *P. glauca* genome, accurate CCS data were assembled using hifiasm (version 0.16)[63]. Next, purge_dups (version 1.2.6)[64] was used to reduce the number of heterozygous duplications. The chromosome-linking steps were identical to those used for the *O. kenojei* genome. Finally, the completeness assessment of assembled genomes was conducted using BUSCO based on the metazoa odb10 dataset and the Core Vertebrate Genes[65] in gVolante (https://gvolante.riken.jp/).

Genome annotation

For genome repeat annotation, we first used RepeatModeler (version 1.0.8) and LTR-FINDER (version 1.0.6)[66] to construct a custom repeat library and then used RepeatMasker (version 4.0.6)[67] to search the genome repeats against both our custom library and Repbase (version 21.01) database by using the following parameters: -nolow -no_is -norna -engine ncbi. RepeatProteinMask (version 4.0.6) was also used for perform homolog-based search at the protein level with the following parameters: -engine ncbi -noLowSimple -p-value 0.0001. In addition, tandem repeats were detected using Tandem Repeats Finder (version 4.07)[68] with the following parameters: -Match 2 -Mismatch 7 -Delta 7 -PM 80 -PI 10 -Minscore 50 -MaxPeriod 2000. Next, by using the aforementioned method, we detected repeat contents in other cartilaginous fishes for downstream analysis (Supplementary Table 8).

For gene annotation, protein sequences of *Chiloscyllium punctatum*, *S. torazame*, *Callorhinchus milii*, *Rhincodon typus*, and *Carcharodon carcharias* (Supplementary Table 9) were downloaded from public databases and mapped to the genome using BLAT (version 35.1)[69]. Next, gene models were predicted using GeneWise (version 2.4.1)[70]. RNA reads were aligned to the genome using HISAT2[71]. Furthermore, transcripts were assembled using Stringtie (version 1.2.2)[72], and open reading frames were predicted using TransDecoder (version

https://doi.org/10.1038/s41467-025-62544-w

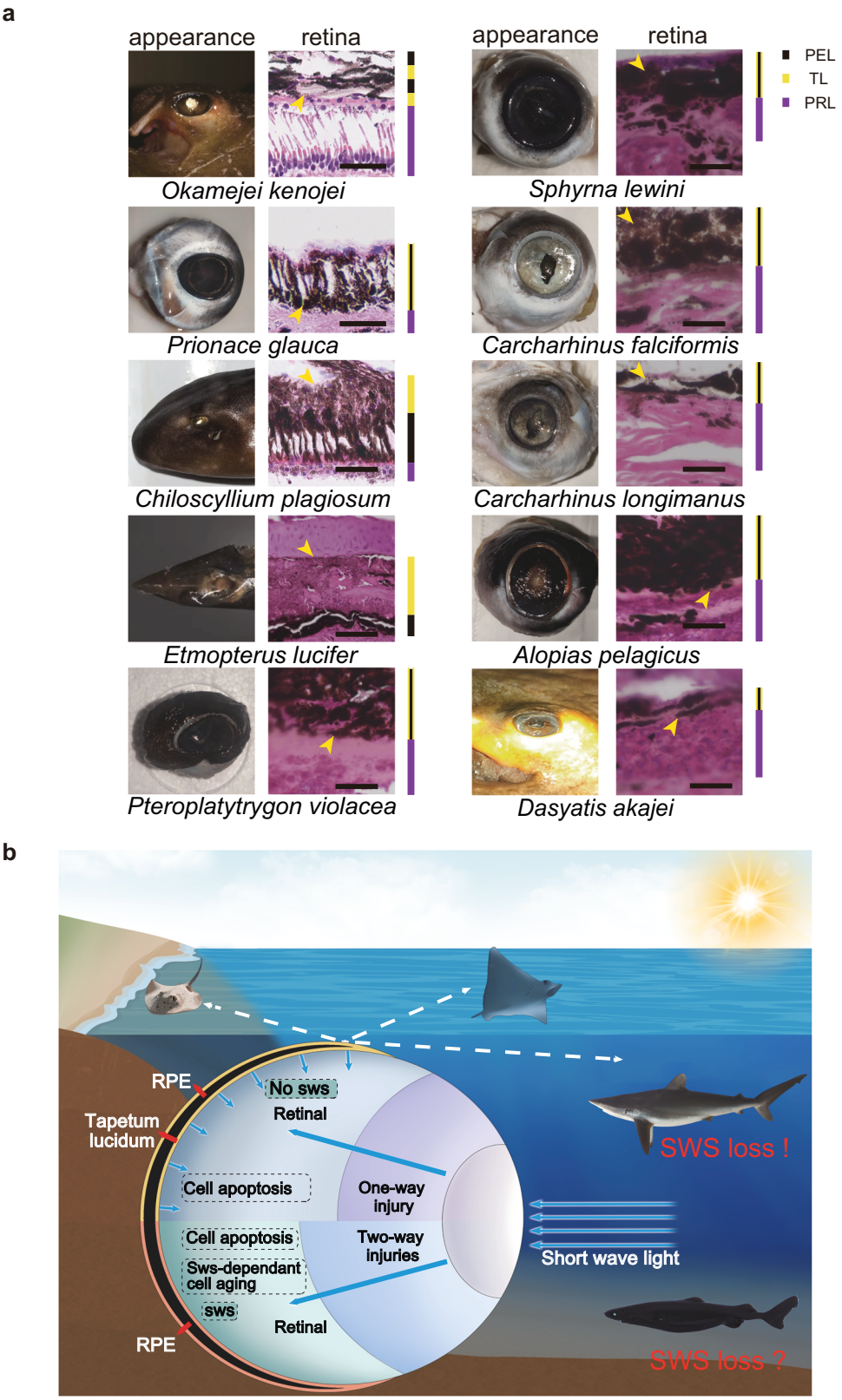

Fig. 5 | Relationship between tapetum lucidum and sws loss in cartilaginous fishes. a Tapetum lucidum (TL) in the eyes of some cartilaginous fishes. The image was taken with a flash in the dark, all fishes were ever frozen except for *Okamejei kenojei* and *Chiloscyllium plagiosum*. Tissue sections show the location of the tapetum lucidum in the pigment epithelial layer (PEL). PRL:photoreceptor cell layer. Scale bar: 50 μm. $n = 1$, the experiment was not repeated and 5 slices were made for each sample, and the best complete slice was selected for display. **b** Simplified model of *sws* loss in cartilaginous fish. The lower half of the eye in the schematic illustrates a two-way retinal injury mechanism, including apoptosis and SWS-dependent cell aging, which is induced by shortwave light in the presence of SWS. The upper half of the eye in the schematic shows that in cartilaginous fish, the tapetum lucidum can reflect shortwave light, thus reducing retinal damage. Thus, with *sws* loss, cartilaginous fish sustain shortwave-light-induced retinal injury only via a one-way mechanism. RPE retinal pigment epithelium.

5.5.0; http://transdecoder.sourceforge.net/). Finally, GLEAN[73] was used to integrate a nonredundant gene set.

For gene function annotation, protein sequences were aligned to sequences from various databases including Swiss-Prot, TrEMBL[74], and KEGG (version 105)[75] by using BLASTP (version 2.2.26)[76]. Function-specific motifs and domains were determined by InterProScan (version 5.60-92.0)[77] according to several protein databases, including Pfam, SMART, PANTHER, PRINTS, PROSITE profiles, and ProSitePatterns. Gene Ontology annotation results were extracted from the InterProScan results. Finally, protein clustering was performed with 70% similarity by using Cd-hit (version 4.8.1)[78].

Gene family analysis

Gene sequences of *Amblyraja radiata*, *Chiloscyllium plagiosum*, *Callorhinchus milii*, *Carcharodon carcharias*, *Chiloscyllium punctatum*, *Rhincodon typus*, *Scyliorhinus torazame*, *Latimeria chalumnae*, *Lepisosteus oculatus*, *Danio rerio*, *Acipenser ruthenus*, *Coilia nasus*, *Gasterosteus aculeatus*, *Takifugu rubripes*, and *Scleropages formosus* were downloaded from the NCBI database (Supplementary Table 10). Next, SonicParanoid[79] was used to identify orthologous groups among the species, and the third base from qualifying codons was then extracted and compiled for all species, resulting in a reduced dataset of four-fold degenerate sites to construct a phylogenetic tree using IQ-TREE[80] with the maximum-likelihood method. The divergence times were inferred on MCMCtree[81], and the calibrating fossil times were searched on TimeTree[22]: *L. chalumnae* and *Le. oculatus*, 424–440 Mya; *L. chalumnae* and *Cal. milii*, 442–515 Mya; *A. ruthenus* and *Le. oculatus*, 345–372 Mya; *Le. oculatus* and *D. rerio*, 298–342 Mya; *Sc. formosus* and *D. rerio*, 244–301 Mya; *Coi. nasus* and *D. rerio*,151–246 Mya; *G. aculeatus* and *T. rubripes*, 82–174 Mya; *Car. carcharias* and *R. typus*, 113–289 Mya; *Cal. milii* and *A. radiata*, 338–471 Mya; and *C. plagiosum* and *A. radiata*, 245–343 Mya. The expansion and contraction of gene families were then defined using CAFE (version 5.0)[82] using the base model, and the clade_and_size_filter.py script from the CAFE package was used to filter out gene families with copy numbers exceeding 100 in one or more species to avoid noninformative parameter estimates. In order to verify identify representative expanded gene families, we used miniprot (version 0.12)[83] to align reference proteins from pathway in KEGG database to target genomes, obtaining combined homolog results with the genewise results. Multiple animo acid sequences alignments were generated using MAFFT (v7.407)[84] and the gene trees were constructed by FastTree (2.1.10)[85] using maximum likelihood method.

Opsin gene identification

Protein sequences of cartilaginous fishes and reference opsin genes of 24 species were downloaded from NCBI and published articles (Supplementary Table 11). Then, the opsin genes from NCBI databases (Supplementary Data 8) were aligned with the whole-protein sequences by using BLASTP (version 2.2.26) with the following parameters: -e 1e-5. For *Raja brachyura*, *M. birostris*, and *S. acanthias* (the annotation information of which was unavailable), we used miniprot (version 0.12)[83] to align opsin proteins with their genomes and obtain opsin homologs.

Zebrafish

Here, we used AB WT zebrafish procured from the Shanghai Institute of Biochemistry and Cell Biology, Chinese Academy of Sciences, China; they were maintained under a 14-h light–10-h dark cycle and fed *Artemia nauplii* twice daily. Embryos were cultivated at a consistent temperature of 27 °C ± 1 °C in egg water, formulated by diluting artificial seawater in regular water at a ratio of 1.5:1000. The zebrafish broodstock was selectively paired at a 1:1 male-to-female ratio[86]. All zebrafish used in this study were anaesthetized with MS-222 before sampling.

Light exposure

For violet light exposure experiments, 10 *sws1*$^{-/-}$ zebrafish and 10 WT zebrafish (all 15 days post fertilization, dpf) were grouped into three parallel groups. All fish were placed in a dark room with violet LED lamps on the top and fed twice per day (in the morning and evening). The water was changed daily, and a 14-h light–10-h dark irradiation cycle was used. The sustained light stimulation time was 30 days. LED lamp wavelength (λ_{max}) and intensity were set to 370 nm and 2,000 ± 100 lx, respectively. For blue light exposure experiments, we followed identical steps but with the following exceptions: *sws1*$^{-/-}$ zebrafish were replaced by *sws2*$^{-/-}$ zebrafish, and λ_{max} was set to 420 nm.

Moreover, zebrafish *sws1*-overexpressing HEK293 cells were cultured under 370-nm violet light for 30 min, whereas zebrafish *sws2*- and human *sws*-overexpressing HEK293 cells were cultured under 420-nm blue light for 30 min; in both experiments, the light intensity was set to 2000 ± 100 lx.

Tissue section preparation

Whole zebrafish (45 dpf) were euthanized and immediately placed in 4% paraformaldehyde for overnight fixation. Next, the specimens were subjected to wash and dehydration steps in an ethanol series at increasing concentrations (75%, 85%, 95%, and 100%; every 30 min). Subsequently, the samples were rendered transparent using xylene, followed by overnight immersion in paraffin. Finally, the paraffin-embedded tissue sample blocks were sectioned into 5-µm-thick slices by using a blade, mounted on gelatin-coated slides, and air-dried.

Hematoxylin and eosin (HE) staining

The paraffin-embedded sections were deparaffinized at 65 °C and rehydrated using an ethanol series at decreasing concentrations (100%, 95%, 90%, 80%, and 70%; every 2 min). Subsequently, they were immersed in a hematoxylin dye solution for 5 min, followed by rinsing with running water. To enable differentiation, we immersed the sections in a 0.5% hydrochloric acid–alcohol solution for 10 s, followed by rinsing under running water and immersion in a 1% eosin dye solution for 10 s. After gradient dehydration, the sections were exposed to xylene for 1–2 min to develop transparency. Finally, the sections were mounted with resin. For each zebrafish sample, the paraffin section with the largest cross-section of the lens was selected for staining treatment, and the images of the dorsal and ventral center of the retina were selected for statistical and analysis of cell number and cell length. The staining results were recorded with a pathology slide scanner (SQS12P, TEKSORAY, CN).

Immunohistochemically staining

The tissue sections were placed in 3% hydrogen peroxide, followed by incubation at room temperature for 25 min in the dark and then by three phosphate-buffered saline (PBS) washings with shaking for 5 min. Next, 3% bovine serum albumin (BSA) was added to cover the tissue section evenly and air-dried at room temperature for 30 min. Next, the BSA seal was removed, and primary antibodies (IL6 Rabbit mAb, ABclonal, Catlog NO.:A22222 at 1:200 dilution; Anti-Caspase-3 Rabbit pAb(Servicebio,Catalog NO.:GB11009-1 at 1:100 dilution) suspended in PBS were added to the sections. All sections were then placed flat in a wet box and incubated at 4 °C overnight; this was followed by three PBS washings with shaking for 5 min. After the slices dried slightly, the sections were incubated with corresponding horseradish peroxidase-labeled corresponding secondary antibodies (HRP IgG, Servicebio, Catalog NO.:GB23303 at 1:200 dilution) at room temperature for 50 min, followed by three PBS washings with shaking for 5 min After the sections dried slightly, the freshly prepared a DAB color-developing solution was added to the section. Next, the sections were covered with hematoxylin dye solution for 3 min, followed by rinsing under running water. After another gradient dehydration, the

sections were exposed to xylene for 1–2 min to increase their transparency. Finally, the slices were mounted using resin. The staining results were recorded with a pathology slide scanner (DS-Ri2, Nikon, Japan).

Immunofluorescence

All paraffin-embedded tissue sections used here were treated similarly to the sections used for immunohistochemical staining until the secondary antibody addition step. After washing off the secondary antibodies, we incubated the sections with DAPI at room temperature for 10 min in the dark to stain the nuclei. Finally, the sections were sealed with an anti-fluorescence quenching agent. The staining results were recorded with a pathology slide scanner (SQS12P, TEKSORAY, CN).

For cell immunofluorescence, cells grown on coverslips were fixed with 4% ice-cold paraformaldehyde PBS for 20 min, followed by treatment with 0.1% TritonX-100 PBS for 10 min. After washing the sections with PBS twice, we blocked the cells with 5% BSA at 37 °C for 30 min and then incubated them with primary antibodies (CDKN2A/p16INK4a Rabbit mAb, ABclonal, Catalog NO.:A11651 at 1:200 dilution) at 4 °C overnight. Next, the cells were washed with PBS and incubated with the corresponding secondary antibodies (ABflo 488-conjugated Goat Anti-Rabbit IgG(H + L), ABclonal, Catalog NO.:AS053 at 1:500 dilution) at 37 °C for 30 min. Finally, DAPI was used to stain the nuclei, and the sections were sealed with an anti-fluorescence quenching agent. The staining results were recorded with a pathology slide scanner (SP8, Leica, Germany).

TUNEL staining

TUNEL assay kit (E-CK-A331, Elabscience, US) and TMB chromogenic (322550, ACD, US) were performed for TUNEL staining according to the kit instructions. The paraffin sections were routinely dewaxed and rehydrated, followed by washing with PBS. Subsequently, the repair solution containing proteinase K from the kit was added and incubated at 37 °C in a humid chamber for 1 h. After washing with PBS, the balance solution from the kit was applied and equilibrated at 37 °C in a humid chamber for 30 min.

Following this, the TdT enzyme and HRP-dUTP mixed working solution were prepared according to the instructions provided in the kit. The buffer on the sections was removed by centrifugation before adding the prepared mixed working solution, which was then incubated at 37 °C in a humid chamber for 1 h. After another wash with PBS, the TMB chromogenic substrate was added and allowed to stand at room temperature for 5 min. Finally, observations were made under a light microscope; a blue-green coloration indicated a positive signal. The staining results were recorded with a pathology slide scanner (SQS12P, TEKSORAY, CN).

Total RNA extraction and cDNA synthesis from zebrafish eyes

Three zebrafish eye tissue samples were collected, and RNA extraction was performed according to the protocol outlined in the RNA isoPlus specification (9108; Takara, Japan). Subsequently, first-strand cDNA was synthesized using a HiSlid cDNA Synthesis Kit (MKG840; MIKX, China), according to the manufacturer's instructions.

RNA sequencing analysis

We obtained three mixed samples of zebrafish eye tissue from each of the following groups: normally fed WT, blue-light–exposed WT, violet-light–exposed WT, blue-light–exposed *sws2*$^{-/-}$ mutant, and violet-light–exposed *sws1*$^{-/-}$ mutant. Sequencing was conducted at Shanghai Ouyi Biology. Differential expression analysis was performed using DESeq2, with Q value < 0.05 and fold change > 2 or fold change <0.5 set as the thresholds for significantly differentially expressed genes.

qRT-PCR

We performed RT-qPCR by using the Pro SYBR qPCR Mix (MKG800; MIKX, China). Specifically, divergent primers annealing at the distal ends of circRNA were used to quantify circRNA abundance. Supplementary Table 12 provides the details of the RT-qPCR primers used. Amplification was performed on a StepOnePlus Real-Time PCR System (CFX; Bio-Rad, USA), and Ct thresholds were determined using the relevant software program.

Zebrafish gene editing based on CRISPR/Cas9 system

Knockout targets for zebrafish *sws1* and *sws2* were designed in The University of California Santa Cruz Genome Browser (https://genome.ucsc.edu/). The sgRNA and *cas9* mRNA synthesized in vitro were microinjected into WT zebrafish embryos. These embryos were cultured to the age of 3 months, and F0 generation heterozygous mutants were screened through Sanger sequencing. Heterozygous and WT zebrafish were then used to obtain F1 zebrafish, and homozygous mutants were screened through Sanger sequencing (Supplementary Fig. 8)[87]. All sequencing was performed at Shanghai Sangong Biological Company.

Behavioral testing

We performed behavioral testing to evaluate *sws1* and *sws2* knockout in zebrafish by using the Y-maze experiment (20 cm × 50 cm arm length); the three arms of the Y-maze were set as the starting, light, and dark arms. Equal amounts of feed were provided in the light and dark arms. In total, 30 WT and 30 mutant zebrafish were assessed consecutively. Each fish was tested for 2 min, starting from the starting arm, three times. The final swimming direction was recorded.

Vector construction and transfection

To construct an opsin overexpression plasmid, we cloned human *sws*, zebrafish *sws1*, and *sws2* cDNAs into the pmcherry-N1 vector using the Homologous Recombinant Kit (C113; Vazyme; Supplementary Fig. 9a). Primers used for amplification are listed in Supplementary Table 12. The plasmid was transfected into HEK293 cells by using Lipo8000 (C0533FT; Beyotime, USA), according to the manufacturer's instructions. In order to construct a stable cell line, the transfected cells were transferred to 10 cm dish, and 800 ng/μl of G418 was added for screening, and the monoclonal cell line was obtained and cultured into a stable cell line. Fluorescence signals were observed under a fluorescence microscope (IX53; Olympus, Japan). Untransfected HEK293 cells and pmcherry-N1 transfected cells were used as controls.

SA-β-gal staining

For SA-β-gal staining, we used the SA-β-Gal Staining Kit (G1073; Servicebio, China), according to the manufacturer's instructions. Synovial cells were fixed with senescent cell staining fixative for 15 min and washed three times, followed by incubation in SA-β-gal staining solution at 37 °C for 24 h. Images were captured under an inverted fluorescence microscope, and SA-β-gal-positive synovial cells were randomly divided into three regions.

Statistical analysis

All data in this study are expressed as means ± standard deviations. Analyses were performed on Prism (version 9.1.2; GraphPad Software). The means of the groups were compared using a Student's *t* test and analysis of variance. *P* values were calculated using a log-rank test, and $P < 0.05$ was considered to indicate statistical significance.

Reporting summary

Further information on research design is available in the Nature Portfolio Reporting Summary linked to this article.

Data availability

O. kenojei data supporting the current findings have been deposited in the CNGB Sequence Archive[88] of China National GeneBank DataBase[89] (accession no.: CNP0003537) and at NCBI (BioProject no.: PRJNA990959). The genome assembly, annotation files, and all the sequencing data of *P. glauca* have been deposited at NCBI (BioProject no.: PRJNA1018302; BioSample no.: SAMN37447395[https://www.ncbi.nlm.nih.gov/biosample?LinkName=bioproject_biosample_all&from_uid=1018302]). The *O. kenojei* and *P. glauca* Genome Shotgun projects have also been deposited in the DDBJ/ENA/GenBank (accession nos.: JAVHYY000000000.1 [https://www.ncbi.nlm.nih.gov/nuccore/JAVHYY000000000] and JBBMRE000000000, respectively). The GenBank assembly versions of *O. kenojei* and *P. glauca* described herein are GCA_035221665.1 [https://www.ncbi.nlm.nih.gov/datasets/genome/GCA_035221665.1/] and GCA_037974335.1 [https://www.ncbi.nlm.nih.gov/datasets/genome/GCA_037974335.1/], respectively. Source data are provided with this paper.

References

1. Collin, S. P. et al. Ancient colour vision: multiple opsin genes in the ancestral vertebrates. *Curr. Biol.* **13**, R864–R865 (2003).
2. Renz, A., Meyer, A. & Kuraku, S. Revealing less derived nature of cartilaginous fish genomes with their evolutionary time scale inferred with nuclear genes. *PLoS ONE***8**, e66400 (2013).
3. Hart, N., Lisney, T., Marshall, N. & Collin, S. Multiple cone visual pigments and the potential for trichromatic color vision in two species of *elasmobranch*. *J. Exp. Biol.* **207**, 4587–4594 (2005).
4. Theiss, S. M., Lisney, T. J., Collin, S. P. & Hart, N. S. Colour vision and visual ecology of the blue-spotted maskray, *Dasyatis kuhlii* Müller & Henle, 1814. *J. Comp. Physiol.* **193**, 67–79 (2007).
5. Bedore, C. N. et al. A physiological analysis of color vision in batoid *elasmobranchs*. *J. Comp. Physiol.* **199**, 1129–1141 (2013).
6. Van-Eyk, S. M., Siebeck, U. E., Champ, C. M., Marshall, J. & Hart, N. S. Behavioural evidence for colour vision in an elasmobranch. *J. Exp. Biol.* **214**, 4186–4192 (2011).
7. Ripps, H. & Dowling, J. E. Structural features and adaptive properties of photoreceptors in the skate retina. *J. Exp. Zool.* **5**, 46–54 (1990).
8. Venkatesh, B. et al. Elephant shark genome provides unique insights into gnathostome evolution. *Nature* **505**, 174–179 (2014).
9. Read, T. D. et al. Draft sequencing and assembly of the genome of the world's largest fish, the whale shark: *Rhincodon typus*. *BMC Genom.* **18**, 532 (2017).
10. Hara, Y. et al. Shark genomes provide insights into elasmobranch evolution and the origin of vertebrates. *Nat. Ecol. Evol.* **2**, 1761–1771 (2018).
11. Shapiro, J. A. & von Sternberg, R. J. B. R. Why repetitive DNA is essential to genome function. *Biol. Rev.* **80**, 227–250 (2005).
12. Marra, N. J. et al. White shark genome reveals ancient *elasmobranch* adaptations associated with wound healing and the maintenance of genome stability. *Proc. Natl. Acad. Sci. USA* **116**, 4446–4455 (2019).
13. Zhang, Y. et al. The white-spotted bamboo shark genome reveals chromosome rearrangements and fast-evolving immune genes of cartilaginous fish. *iScience* **23**, 101754 (2020).
14. Clark, K. J., Carlson, D. F., Leaver, M. J., Foster, L. K. & Fahrenkrug, S. C. Passport, a native Tc1 transposon from flatfish, is functionally active in vertebrate cells. *Nucleic Acids Res.* **37**, 1239–1247 (2009).
15. Robert, V. J. & Bessereau, J.-L. J. G. Manipulating the *Caenorhabditis elegans* genome using mariner transposons. *Genetica* **138**, 541–549 (2010).
16. Horie, K. et al. Efficient chromosomal transposition of a Tc1/mariner-like transposon Sleeping Beauty in mice. *Proc. Natl. Acad. Sci. USA* **98**, 9191–9196 (2001).
17. Bradic, M., Warring, S. D., Low, V. & Carlton, J. M. J. M. D. The Tc1/mariner transposable element family shapes genetic variation and gene expression in the protist Trichomonas vaginalis. *Mob. DNA* **5**, 1–11 (2014).
18. Shen, D. et al. A native, highly active Tc1/mariner transposon from zebrafish (ZB) offers an efficient genetic manipulation tool for vertebrates. *Nucleic Acids Res.* **49**, 2126–2140 (2021).
19. Wodarz, A. & Nusse, R. Mechanisms of Wnt signaling in development. *Annu. Rev. Cell Dev. Biol.* **14**, 59–88 (1998).
20. Liu, J. et al. Wnt/beta-catenin signalling: function, biological mechanisms, and therapeutic opportunities. *Signal Transduct. Tar.* **7**, 3 (2022).
21. Marletaz, F. et al. The little skate genome and the evolutionary emergence of wing-like fins. *Nature* **616**, 495–503 (2023).
22. Kumar, S. et al. TimeTree 5: An expanded resource for species divergence times. *Mol. Biol. Evol.* **39**, https://doi.org/10.1093/molbev/msac174 (2022).
23. Licht, M. et al. Contribution to the molecular phylogenetic analysis of extant holocephalan fishes (*Holocephali*, *Chimaeriformes*). *Org. Divers Evol.* **12**, 421–432 (2012).
24. Fernández, R. & Gabaldón, T. Gene gain and loss across the metazoan tree of life. *Nat. Ecol. Evol.* **4**, 524–533 (2020).
25. Domazet-Lošo, M., Široki, T., Šimičević, K. & Domazet-Lošo, T. Macroevolutionary dynamics of gene family gain and loss along multicellular eukaryotic lineages. *Nat. Commun.* **15**, 2663 (2024).
26. Tan, M. et al. The whale shark genome reveals patterns of vertebrate gene family evolution. *eLife* **10**, https://doi.org/10.7554/eLife.65394 (2021).
27. Craig, Z. R. *Encyclopedia of Reproduction (Second Edition)* (ed Skinner, M. K.) 707-713 (Academic Press, 2018).
28. Ebert, D. A., Fowler, S., Compagno, L. & Dando, M. *Sharks of The World: A Fully Illustrated Guide* (Wild Nature Press, 2021).
29. Prucha, M. S. et al. Steroidogenic acute regulatory protein transcription is regulated by estrogen receptor signaling in largemouth bass ovary. *Gen. Comp. Endocrinol.* **286**, 113300 (2020).
30. Nunez, B. S. & Evans, A. N. Hormonal regulation of the steroidogenic acute regulatory protein (StAR) in gonadal tissues of the Atlantic croaker (*Micropogonias undulatus*). *Gen. Comp. Endocrinol.* **150**, 495–504 (2007).
31. Trezise, A. E. & Collin, S. P. Opsins: evolution in waiting. *Curr. Biol.* **15**, R794–R796 (2005).
32. Tosini, G., Ferguson, I. & Tsubota, K. Effects of blue light on the circadian system and eye physiology. *Mol. Vis.* **22**, 61–72 (2016).
33. Cougnard-Gregoire, A. et al. Blue light exposure: ocular hazards and prevention-a narrative review. *Ophthalmol. Ther.* **12**, 755–788 (2023).
34. Zekavat, S. M. et al. Photoreceptor layer thinning is an early biomarker for age-related macular degeneration: epidemiologic and genetic evidence from UK biobank OCT data. *Ophthalmology* **129**, 694–707 (2022).
35. Mainster, M. A. Violet and blue light blocking intraocular lenses: photoprotection versus photoreception. *Br. J. Ophthalmol.* **90**, 784–792 (2006).
36. Margrain, T. H., Boulton, M., Marshall, J. & Sliney, D. H. Do blue light filters confer protection against age-related macular degeneration?. *Prog. Retin. Eye Res.* **23**, 523–531 (2004).
37. Shao, F., Han, M. & Peng, Z. Evolution and diversity of transposable elements in fish genomes. *Sci. Rep.* **9**, 15399 (2019).
38. Richter, D. J., Fozouni, P., Eisen, M. B. & King, N. Gene family innovation, conservation and loss on the animal stem lineage. *Elife* **7**, e34226 (2018).
39. Guijarro-Clarke, C., Holland, P. W. H. & Paps, J. Widespread patterns of gene loss in the evolution of the animal kingdom. *Nat. Ecol. Evol.* **4**, 519–523 (2020).
40. Yamaguchi, K., Koyanagi, M. & Kuraku, S. Visual and nonvisual opsin genes of sharks and other nonosteichthyan vertebrates: genomic

exploration of underwater photoreception. *J. Evol. Biol.* **34**, 968–976 (2021).
41. Davies, W. L. et al. Into the blue: gene duplication and loss underlie color vision adaptations in a deep-sea chimaera, the elephant shark *Callorhinchus milii*. *Genome Res* **19**, 415–426 (2009).
42. Albalat, R. & Cañestro, C. Evolution by gene loss. *Nat. Rev. Genet.* **17**, 379–391 (2016).
43. Xu, P. et al. Draft genome of the mirrorwing flyingfish (*Hirundichthys speculiger*). *Front. Genet.* **12**, 695700 (2021).
44. Simões, B. F. et al. As blind as a bat? Opsin phylogenetics illuminates the evolution of color vision in bats. *Mol. Biol. Evol.* **36**, 54–68 (2019).
45. Guinot, G. & Condamine, F. L. Global impact and selectivity of the Cretaceous-Paleogene mass extinction among sharks, skates, and rays. *Science* **379**, 802–806 (2023).
46. Sibert, E. C. & Rubin, L. D. An early Miocene extinction in pelagic sharks. *Science* **372**, 1105–1107 (2021).
47. Hart, N. S. et al. Visual opsin diversity in sharks and rays. *Mol. Biol. Evol.* **37**, 811–827 (2020).
48. Lisney, T., Theiss, S., Collin, S. & Hart, N. Vision in *elasmobranchs* and their relatives: 21st century advances. *J. Fish. biol.* **80**, 2024–2054 (2012).
49. Litherland, L., Collin, S. P. & Fritsches, K. A. Visual optics and ecomorphology of the growing shark eye: a comparison between deep and shallow water species. *J. Exp. Biol.* **212**, 3583–3594 (2009).
50. Vee, S., Barclay, G. & Lents, N. H. The glow of the night: the tapetum lucidum as a co-adaptation for the inverted retina. *Bioessays* **44**, e2200003 (2022).
51. Protas, M. E. et al. Genetic analysis of cavefish reveals molecular convergence in the evolution of albinism. *Nat. Genet.* **38**, 107–111 (2006).
52. Lin, Q. et al. The seahorse genome and the evolution of its specialized morphology. *Nature* **540**, 395–399 (2016).
53. Olson, M. V. When less is more: gene loss as an engine of evolutionary change. *Am. J. Hum. Genet.* **64**, 18–23 (1999).
54. Olson, M. V. & Varki, A. Sequencing the chimpanzee genome: insights into human evolution and disease. *Nat. Rev. Genet.* **4**, 20–28 (2003).
55. Schwab, I. R., Yuen, C. K., Buyukmihci, N. C., Blankenship, T. N. & Fitzgerald, P. G. Evolution of the tapetum. *Trans. Am. Ophth. Soc.* **100**, 187–199 (2002).
56. McBride, C. S., Arguello, J. R. & O'Meara, B. C. Five Drosophila genomes reveal nonneutral evolution and the signature of host specialization in the chemoreceptor superfamily. *Genetics* **177**, 1395–1416 (2007).
57. Hecker, N., Sharma, V. & Hiller, M. Transition to an aquatic habitat permitted the repeated loss of the pleiotropic *KLK8* gene in mammals. *Genome Biol. Evol.* **9**, 3179–3188 (2017).
58. Mak, S. S. T. et al. Comparative performance of the BGISEQ-500 vs Illumina HiSeq2500 sequencing platforms for palaeogenomic sequencing. *GigaScience* **6**, 1–13 (2017).
59. Liu, H., Wu, S., Li, A. & Ruan, J. SMARTdenovo: a de novo assembler using long noisy reads. *GigaByte* **2021**, gigabyte15 (2021).
60. Walker, B. J. et al. Pilon: an integrated tool for comprehensive microbial variant detection and genome assembly improvement. *PLoS ONE***9**, e112963 (2014).
61. Durand, N. C. et al. Juicer provides a one-click system for analyzing loop-resolution Hi-C experiments. *Cell Syst.* **3**, 95–98 (2016).
62. Dudchenko, O. et al. De novo assembly of the Aedes aegypti genome using Hi-C yields chromosome-length scaffolds. *Science* **356**, 92–95 (2017).
63. Cheng, H., Concepcion, G. T., Feng, X., Zhang, H. & Li, H. Haplotype-resolved de novo assembly using phased assembly graphs with hifiasm. *Nat. Methods* **18**, 170–175 (2021).
64. Guan, D. et al. Identifying and removing haplotypic duplication in primary genome assemblies. *Bioinformatics* **36**, 2896–2898 (2020).
65. Nishimura, O., Hara, Y. & Kuraku, S. gVolante for standardizing completeness assessment of genome and transcriptome assemblies. *Bioinformatics* **33**, 3635–3637 (2017).
66. Xu, Z. & Wang, H. LTR_FINDER: an efficient tool for the prediction of full-length LTR retrotransposons. *Nucleic Acids Res.* **35**, W265–W268 (2007).
67. Tarailo-Graovac, M. & Chen, N. Using RepeatMasker to identify repetitive elements in genomic sequences. *Current Protocols in Bioinformatics Ch. 4* https://doi.org/10.1002/0471250953.bi0410s25 (2009).
68. Benson, G. Tandem repeats finder: a program to analyze DNA sequences. *Nucleic Acids Res.* **27**, 573–580 (1999).
69. Kent, W. J. BLAT-the BLAST-like alignment tool. *Genome Res.* **12**, 656–664 (2002).
70. Madeira, F. et al. Search and sequence analysis tools services from EMBL-EBI in 2022. *Nucleic Acids Res.* **50**, W276–W279 (2022).
71. Kim, D., Paggi, J. M., Park, C., Bennett, C. & Salzberg, S. L. Graph-based genome alignment and genotyping with HISAT2 and HISAT-genotype. *Nat. Biotechnol.* **37**, 907–915 (2019).
72. Pertea, M., Kim, D., Pertea, G. M., Leek, J. T. & Salzberg, S. L. Transcript-level expression analysis of RNA-seq experiments with HISAT, StringTie and Ballgown. *Nat. Protoc.* **11**, 1650–1667 (2016).
73. Elsik, C. G. et al. Creating a honey bee consensus gene set. *Genome Biol.* **8**, R13 (2007).
74. Bairoch, A. & Apweiler, R. The SWISS-PROT protein sequence database and its supplement TrEMBL in 2000. *Nucleic Acids Res.* **28**, 45–48 (2000).
75. Kanehisa, M., Furumichi, M., Sato, Y., Kawashima, M. & Ishiguro-Watanabe, M. KEGG for taxonomy-based analysis of pathways and genomes. *Nucleic Acids Res.* **51** https://doi.org/10.1093/nar/gkac963 (2022).
76. Altschul, S. F., Gish, W., Miller, W., Myers, E. W. & Lipman, D. J. Basic local alignment search tool. *J. Mol. Biol.* **215**, 403–410 (1990).
77. Zdobnov, E. M. & Apweiler, R. InterProScan-an integration platform for the signature-recognition methods in InterPro. *Bioinformatics* **17**, 847–848 (2001).
78. Li, W. & Godzik, A. Cd-hit: a fast program for clustering and comparing large sets of protein or nucleotide sequences. *Bioinformatics* **22**, 1658–1659 (2006).
79. Cosentino, S. & Iwasaki, W. SonicParanoid: fast, accurate and easy orthology inference. *Bioinformatics* **35**, 149–151 (2019).
80. Nguyen, L. T., Schmidt, H. A., von Haeseler, A. & Minh, B. Q. IQ-TREE: a fast and effective stochastic algorithm for estimating maximum-likelihood phylogenies. *Mol. Biol. Evol.* **32**, 268–274 (2015).
81. Yang, Z. PAML 4: phylogenetic analysis by maximum likelihood. *Mol. Biol. Evol.* **24**, 1586–1591 (2007).
82. Mendes, F. K., Vanderpool, D., Fulton, B. & Hahn, M. W. CAFE 5 models variation in evolutionary rates among gene families. *Bioinformatics* **36**, 5516–5518 (2020).
83. Li, H. Protein-to-genome alignment with miniprot. *Bioinformatics* **39**, https://doi.org/10.1093/bioinformatics/btad014 (2023).
84. Katoh, K. & Standley, D. M. MAFFT multiple sequence alignment software version 7: improvements in performance and usability. *Mol. Biol. Evol.* **30**, 772–780 (2013).
85. Price, M. N., Dehal, P. S. & Arkin, A. P. FastTree 2-approximately maximum-likelihood trees for large alignments. *PLoS ONE***5**, e9490 (2010).
86. Nasiadka, A. & Clark, M. D. Zebrafish breeding in the laboratory environment. *ILAR J.* **53**, 161–168 (2012).
87. Varshney, G. K. et al. A high-throughput functional genomics workflow based on CRISPR/Cas9-mediated targeted mutagenesis in zebrafish. *Nat. Protoc.* **11**, 2357–2375 (2016).

88. Guo, X. et al. CNSA: a data repository for archiving omics data. *Database-OXFORD* **2020**, https://doi.org/10.1093/database/baaa055 (2020).
89. Chen, F. Z. et al. CNGBdb: China national geneBank database. *Yi Chuan* **42**, 799–809 (2020).

Acknowledgements

We sincerely thank Bilin Liu for providing eye sample of *Pteroplatytrygon violacea*, and Sheng Li, Linlin Zhang and Hua Bai for their insightful discussion. We sincerely thank Mr. Pan Liu for providing the images of *Zameus squamulosus* and *Carcharhinus falciformis*. This study was supported by the National Natural Science Foundation of China [grant numbers 31872546 for B.B., 42276092 for Yunkai Li], the Tianjin Natural Science Foundation [grant number 17JCQNJC15000 for B.Z.], the Transformation Project of Tianjin Agricultural Achievements [grant number 201604090 for B.Z.], the Special Funding for Modern Agricultural Industrial Technology System [grant number CARS-47-Z01 for L.J.], the Modern Industrial Technology System in Tianjin [grant number ITTFRS2017011 for B.Z.], the Program for Professor of Special Appointment (Eastern Scholar) at Shanghai Institutions of Higher Learning for Yunkai Li.

Author contributions

B.Z. and Y.L. (Yunkai Li) initiated, managed, and led genome sequencing project. B.B., B.Z., N.Z., Y.Z. and J.S. conceived the study. B.B, B.Z, and Y.L. (Yunkai Li) designed the analysis. B.Z. and X.X. prepared the samples. M.L., L.J. and X.X performed the genome assembly and annotation. M.L. and L.J. conducted the gene family and positive selection analysis. Y.F. and Y.L. (Yumin Li) carried out the experiments and data analysis. B.B., B.Z., Y.L. (Yongguan Liao), L.J., Y.F, N.Z., M.L., X.X. and A.M. discussed the data. All authors contributed to data interpretation. B.B., B.Z., M.L., G.F, Y.F., Y.L. (Yunkai Li) and N.Z. wrote and revised the paper, with significant contributions from all other authors.

Competing interests

The authors declare no competing interests.

Additional information

Supplementary information The online version contains supplementary material available at https://doi.org/10.1038/s41467-025-62544-w.

Correspondence and requests for materials should be addressed to Yaolei Zhang, Na Zhao, Yunkai Li or Baolong Bao.

Peer review information *Nature Communications* thanks Leah Campbell, and the other, anonymous, reviewers for their contribution to the peer review of this work. A peer review file is available.